Resonant X-ray Enhancement of the Auger Effect in High-*Z* Atoms, Molecules, and Nanoparticles: Potential Biomedical Applications†

Anil K. Pradhan,*,‡,§ Sultana N. Nahar,‡ Maximiliano Montenegro,‡ Yan Yu,|| H. L. Zhang,⊥ Chiranjib Sur,‡,# Michael Mrozik,▽ and Russell M. Pitzer▽

Department of Astronomy, The Ohio State University, Columbus, Ohio 43210, Chemical Physics Program, The Ohio State University, Columbus, Ohio 43210, Department of Radiation Oncology, Thomas Jefferson University, Philadelphia, Pennsylvania 19107, Applied Physics Division, Los Alamos National Laboratory, Los Alamos, New Mexico 87545, High Performance Computing Group, ISL, IBM India, Bangalore 560 071, India, and Department of Chemistry, The Ohio State University, Columbus, Ohio 43210

Received: May 27, 2009; Revised Manuscript Received: July 16, 2009

It is shown that X-ray absorption can be considerably enhanced at resonant energies corresponding to K-shell excitation into higher shells with electron vacancies following Auger emissions in high-*Z* elements and compounds employed in biomedical applications. We calculate Auger resonant probabilities and cross sections to obtain total mass attenuation coefficients with resonant cross sections and detailed resonance structures corresponding to Kα, Kβ, Kγ, Kδ, and Kη complexes lying between 6.4−7.1 keV in iron and 67−80 keV in gold. The basic parameters were computed using the relativistic atomic structure codes and the **R**-matrix codes. It is found that the average enhancement at resonant energies is up to a factor of 1000 or more for associated K → L, M, N, O, P transitions. The resonant energies in high-*Z* elements such as gold are sufficiently high to ensure significant penetration in body tissue, and hence the possibility of achieving X-radiation dose reduction commensurate with resonant enhancements for cancer theranostics using high-*Z* nanoparticles and molecular radiosensitizing agents embedded in malignant tumors. The in situ deposition of X-ray energy, followed by secondary photon and electron emission, will be localized at the tumor site. We also note the relevance of this work to the development of novel monochromatic or narrow-band X-ray emission sources for medical diagnostics and therapeutics.

Introduction

It is well-known that X-rays interact efficiently with high-*Z* elements, and the importance of that fact has been extensivley explored in biomedical physics.[1−7] Many radiosensitized reactive agents are molecular compounds or moieties containing heavy elements, such as bromodeoxyuridine (BUdR), iododeoxyuridine (IUdR), and cisplatin (cis-Pt) with bromine, iodine, and platinum (Z = 35, 53, and 78) respectively. BUdR and IUdR are widely used in medical imaging, cisPt or Cyclo-Pt are utilized in cancer therapy. The high-*Z* elements undergo Auger fluorescence when irradiated by X-rays[3,4] at energies, for example, above the ionization energy of the innermost (K) shell. Radiation induced ionization of atoms can cause DNA strand breakups in malignant cells.[8,9] Low-energy electrons resulting from Auger breakups can cause single and double strand DNA breakups via electron attachment resonances.[10]

Recently, we have proposed a comprehensive scheme for X-ray resonant theranostics (therapy and diagnostics) along these lines.[11] However, while X-ray interaction with heavy elements is well-known, the detailed physical properties of high-*Z* elements are relatively unknown, either experimentally or theoretically. The problem becomes progressively more difficult with *Z*, especially for elements at the high end of the periodic table such as gold, which is finding increasing usage in nanobiotechnology. Gold is generally nonreactive and therefore ideal for constructing nanoparticles for medical use for in vivo treatment. Laboratory experiments using gold nanoparticles injected into mice tumors, and then irradiated with high-energy 140−250 keVp X-rays, have shown considerable reduction in tumor sizes.[12,13] Gold is particularly appropriate for such experiments owing to its nontoxicity and high Z (=79). The nanoparticle form entails sizes from a few to a few tens of nanometers, and in principle they are sufficient to penetrate cell vascula provided the size is <30 nm or so. X-ray irradiation then enhances the radiation dose uptake, with consequent damage to the malignant cells with embedded nanoparticles.

The broad-band radiation sources employed in these experiments are the generally available X-ray generators in medical facilities. They are X-ray sources with energy output in the form of a bremsstrahlung spectrum, and deliver radiation up to the stated peak voltage. The shape of the output bremsstrahlung spectrum extends up to the peak voltage (kVp) between the cathode and the anode of the generating X-ray tube. Most of the flux from traditional X-ray sources covers an extremely broad range, well over half the total energy range, and a maximum around one-third the peak value.[2,14] For example, for a 250 kVp source the X-ray output ranges between 40 and 250 keV photon energies, with a broad maximum around ∼80 keV. Since the Au K-edge E_I(K) = 80.729 keV, a 250 kVp source is capable of ionizing all inner *n*-shells and subshells of the gold atom with L,M,N,O,P edges at approximately 12−14, 3.4−2.2, 0.11−0.9, 0.01−0.11, and 0.0.009 keV, respectively. Of course,

† Part of the "Russell M. Pitzer Festschrift".

* Corresponding author. E-mail: pradhan@astronomy.ohio-state.edu.
‡ Department of Astronomy, The Ohio State University.
§ Chemical Physics Program, The Ohio State University.
|| Thomas Jefferson University.
⊥ LANL.
Present address: IBM India.
▽ Department of Chemistry, The Ohio State University.

10.1021/jp904977z CCC: $40.75
Published on Web 08/27/2009

much higher energy accelerators are also in common medical usage, e.g., those with up to 6 MVp peak voltage and a broad maximum around 2 MeV.

The main problem with using broad-band bremsstrahlung X-ray sources (ordinary devices, accelerators, or CT scanners) is as follows. The low-energy ($\sim$10−30 keV) flux is absorbed by body tissue close to the skin before reaching the desired target (e.g., tumor); at the same time high-energy X-rays (>1 MeV) barely interact with the light elements and compounds, e.g., H_2O in body tissue or even calcium in bone. Therefore, both the low-energy and the high-energy X-rays are inefficient in terms of proper medical use in imaging or therapy. For optimal usage and to obviate unnecessary exposure to healthy tissue the incident X-rays should be in precisely the right energy range, which can be predetermined, commensurate with dosimetric parameters such as depth and shape as well as the particular physical chemistry of the radiosensitizing agents. But relatively high energy X-rays still are needed to ensure sufficient penetration and to minimize photoabsorption, which scales roughly as E^{-3}.[15] With the exception of the K-edges, the photoionization cross section decreases rapidly with energy and the efficiency of radiation absorption diminishes. Therefore, the incident X-rays need to be not only monochromatic but also preselected for maximum interaction cross sections. While it is promising that irradiation and subsequent breakup of high-Z atoms may be a useful tool in cancer theranostics, the precise interaction of X-rays as a function of incident energy and the target atomic structure needs to be studied to understand and improve the techniques and the concepts involved. The primary aim of this paper is to demonstrate, in principle, the theranostical efficacy of monochromatic X-rays with high-Z elements.

But while broad-band X-ray sources are generally used in medical practice, narrow-band or monochromatic X-ray sources such as synchrotron based devices and laser produced plasmas are available.[16−19] The most useful characteristic of these sources is their capability to generate monochromatic beams of high-intensity photon fluxes. Indeed, it is well-known that the output spectra of ordinary X-ray tubes prominently display Kα, Kβ emission lines superimposed on a bremsstrahlung background[2] and can be easily isolated, albeit with lower X-ray fluxes that may still be used for diagnostic imaging. In addition, advances are being made in generating ultrashort K-shell radiation using femtosecond laser pulses impinging on thin solid material.[20] These sources can be utilized not only for basic studies of matter at atomic and molecular scales but also for probing materials at nanoscales for applications to nanotechnology and biomedical imaging and spectroscopy. Large energy deposition in a small target would produce a transient plasma on short time scales. It is of interest to investigate the material properties of such "plasmoids", and to ascertain the related physical constants as a function of the incident X-ray energy and nuclear charge Z all along the Periodic Table, and other extrinsic parameters such as density and size of the targeted material.

However, the relevant atomic and molecular computations are extremely difficult owing to the fact that both the relativistic effects and many-electron correlation effects need to be considered explicitly. Moreover, careful attention needs to be paid to the energy dependence on the incident photon energy, particularly in energy ranges where resonant phenomena occur with large transition probabilities and cross sections. Available cross sections for attenuation of X-rays by the atoms of different elements have been computed using relatively simple atomic physics methods that yield only the background cross sections, as from the online databases at the National Institute for Standards and Technology (NIST: www.nist.gov[15]). For molecular systems containing a given high-Z element, we assume that the dominant X-ray interaction is with that element. In this paper we study K-shell transitions in two elements, Fe and Au, due to resonant X-ray absorption below the K-edge together with numerical simulations of the transmitted radiation.

Theory and Computations

X-ray absorption by neutral atoms is usually taken into account via continuum or the absorption edges for ionization of individual electronic shells. A rise in absorption coefficient can be seen as the energy crosses the subshell thresholds. Calculated photoabsorption cross sections for the inner shells, including the subshell structure, in high-Z elements are available at NIST.[15] The calculation considered no other structure except the jumps at different shell edges. Figure 1 shows these photoelectric attenuation coefficients for high-Z neutral Fe and Au, compared with a low-Z element O. In the following subsections, we explain relevant inner shell absorption and emission processes.

Auger effect and Electron Vacancies. Energy absorption by an inner shell may have several effects, as demonstrated schematically in Figure 2. It illustrates (i) ionization by X-ray photons with energy higher than K-shell ionization energy, $E_\gamma > E_k$, (ii) multiple electron vacancies created by Auger decays from successively higher shells leading to photon emission and/or electron ejections, and (iii) resonant photoexcitation by an external monoenergetic X-ray source. It is easy to see why a relatively large number of electron vacancies will be created in higher shells following even a single K-shell ionization. As an electron from a higher shell decays to a lower shell, it emits a photon (radiative transition) or ejects an electron (radiationless transition) from the same or higher shell creating another vacancy. The number of vacancies therefore approximately doubles in each decay as the atom stabilizes via Auger cascades, ending up with multiple photon emissions and electron ejections. In a high-Z atom with up to O and P shells occupied, up to 20 or more electrons may be released, most with fairly low energies since they are ejected from high-lying shells; these processes are special cases of the Auger effect and are referred to as Coster−Kronig or Super-Coster−Kronig transitions.[2] Electron emissions and vacancies created by nuclear capture processes in radionuclides may also be considered;[6] but in this paper we confine ourselves only to Auger decays following X-ray ionization.

Resonant Absorption. For atomic or molecular ions, many transitions are possible if electron vacancies exist in subshells, thereby allowing for strong dipole upward excitation transitions by incident photons (Figure 2). Radiative attenuation coefficients, or plasma opacity, is greatly enhanced owing to such resonant line transitions in addition to the background continuum shown in Figure 1. We quantify the opacity in units related to the interaction cross section and density, viz. cm^2/g. Figure 3 shows a sample opacity calculated using atomic data from the Opacity Project[21] for an iron plasma in local thermodynamic equilibrium (as in stellar interiors). The calculated opacity is in the high temperature−density regime, $\log T_e\,(\mathrm{K}) = 6.5$ and $\log N_e\,(\mathrm{cm}^{-3}) = 23.0$. The ionization stages correspond to highly ionized L-shell states of Fe ions, from hydrogen-like to fluorine-like. The distribution among ions isoelectronic with H, He, Li, Be, B, C, N, O, and F-like sequences is 1.4×10^{-4}, 4.27×10^{-3}, 4.22×10^{-2}, 1.71×10^{-1}, 3.18×10^{-1}, 2.95×10^{-1}, 1.36×10^{-1}, 3.09×10^{-2}, and 2.93×10^{-3} respectively. Greatly enhanced photoabsorption occurs via a multitude of strong

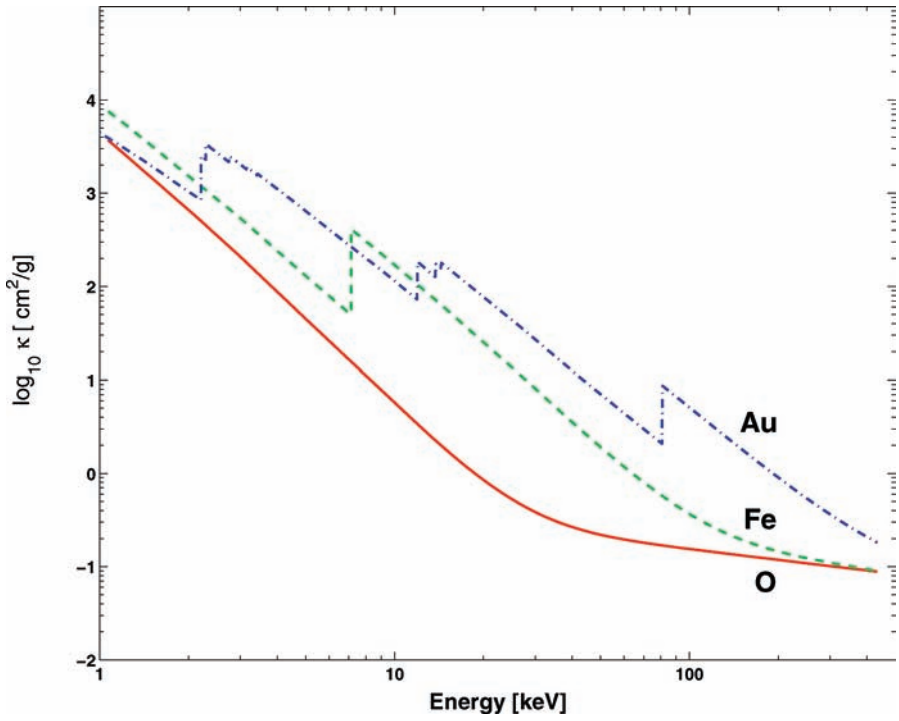

Figure 1. Background photoabsorption attenuation coefficients κ[15] for neutral O, Fe, and Au. The rise in κ at various energies correspond to ionization edges of the K, L, M (sub)shells of Au and the K-shell of Fe. The oxygen K-edge lies at 0.53 keV and is not seen.

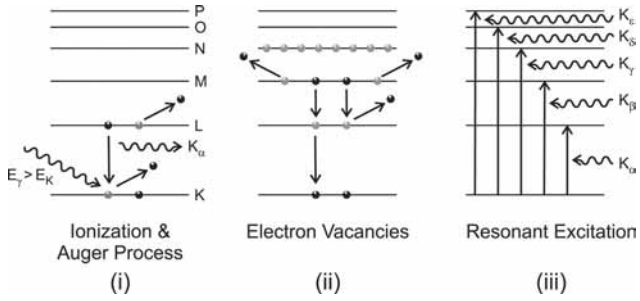

Figure 2. Auger process and resonant excitation: (i) K-shell ionization, Kα emission and/or L-shell Auger electron emission; (ii) multiple electron vacancies created by K-shell ionization due to Auger electron ejections from higher shells and radiative decays; (iii) resonant excitation from the K-shell to higher shells by Kα, Kβ, etc. by incident photons. (The gold atom has electronic shells up to $n = 6$, or the P-shell.)

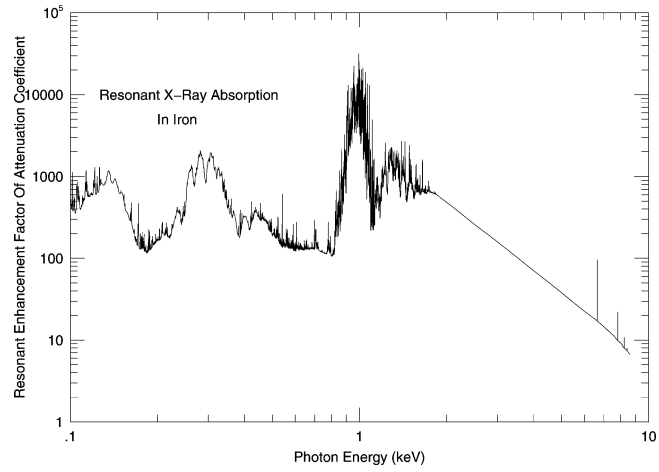

Figure 3. Iron opacity in plasma in local thermodynamic equilibrium in the high temperature−density regime: log T_e = 6.5 K, log N_e = 23.0 cm^{-3} showing a peak absorption or opacity around 1 keV. The opacity was calculated using the codes and atomic data from the Opacity Project.[21,22]

dipole L → M (2p → 3d) transition arrays. A particularly large 1 keV feature is seen to enhance X-ray absorption by several orders of magnitude above the background.

K-shell absorption resonances are not quite as prominent as the multitude of densely packed L-shell resonant features in Figure 3, since there are relatively fewer electrons (only two 1s electrons) involved. But using monochromatic X-ray sources, such as mentioned in the Introduction, resonant excitation from the K-shell into electron vacancies in higher shells may be possible. We examine arrays of Kα transition, 1s → 2p, in the first instance. With vacancies in the L-shell, K-shell electrons may be excited upward via the resonant Kα transitions by incident photons. Such a resonant process would compete with downward decay from higher shells into the L-shell to fill the vacancies. The competing rates depend on the Einstein relation for A coefficient for radiative decay and B coefficient for photon absorption,

$$A_{ji}(\nu) + B_{ji}(\nu)\,\rho_{ij}(\nu) = B_{ij}\rho_{ij}(\nu) \qquad (1)$$

for any two-level system $i \leftrightarrow j$, transition frequency ν, and radiation field density $\rho_{ij}(\nu)$. In the special case of no downward transitions into the K-shell, since it is filled, and therefore no stimulated emission, we can rewrite the B and A coefficients including only radiative transitions from higher n-shells to fill the L-shell vacancy, also competing with upward K-shell excitations. Given the incident photon flux Φ at the resonant energy of Kα,

$$\Phi(\nu_{\mathrm{K}\alpha})g_{\mathrm{K}}B(\mathrm{K}\alpha) = \sum_{n_i>2} g_i A[n_i(S_iL_iJ_i) \rightarrow 2(SLJ)] \qquad (2)$$

where $n_i(S_iL_iJ_i)$ refers to specific fine structure levels of an n-shell, e.g., $2(S_iL_iJ_i)$ refers to the L-shell levels. The fine

TABLE 1: Averaged Kα Resonant Energies and Cross Sections for Fe and Au Ions

			Fe		Au	
ion core	transition array	no. of transitions	$\langle E(\mathrm{K}\alpha)\rangle$ (keV)	$\langle \sigma_{res}(\mathrm{K}\alpha)\rangle$ (Mb)	$\langle E(\mathrm{K}\alpha)\rangle$ (keV)	$\langle \sigma_{res}(\mathrm{K}\alpha)\rangle$ (Mb)
F-like	$1s^22s^22p^5-1s2s^22p^6$	2	6.6444	1.33	68.324	0.99
O-like	$1s^22s^22p^4-1s2s^22p^5$	14	6.5096	5.80	68.713	4.10
N-like	$1s^22s^22p^3-1s2s^22p^4$	35	6.5237	10.12	68.943	5.17
C-like	$1s^22s^22p^2-1s2s^22p^3$	35	6.5633	12.86	69.136	8.63
B-like	$1s^22s^22p^1-1s2s^22p^2$	14	6.5971	7.11	68.938	3.48
Be-like	$1s^22s^2-1s2s^22p$	2	6.6375	5.36	68.889	3.47
Li-like	$1s^22s-1s2s2p$	6	6.6617	5.02	68.893	2.82
He-like	$1s^2-1s2p$	2	6.6930	6.01	68.703	3.93
H-like	$1s-2p$	2	6.9655	2.18	69.663	1.58

structure levels and associated transition rates are given in Nahar et al.[23] The statistical weights of the K-shell and excited levels i are denoted as g_K and g_i respectively. Equation 2 now suggests a *critical photon density* Φ^c such that

$$\Phi^c(\nu_{K\alpha}) = \frac{\sum_{n_i>2} g_i A[n_i(S_iL_iJ_i) \rightarrow 2(SLJ)]}{g_K B_{K\alpha}} \qquad (3)$$

Given a monochromatic Kα photon source of sufficient intensity with $\Phi > \Phi^c$, upward resonant excitations via absorption of Kα photons could occur if L-shell vacancies exist. The radiative decay coefficients for Au are very large,[23] and any vacancy in the L-shell is likely to be filled on a relatively short time scale by a radiative transition from a shell, such as in the transition array $A(\mathrm{M}\rightarrow\mathrm{L}) \approx 10^{14-15}$ s^{-1}. However, the A coefficients for the Kα transitions L → K are even higher $\approx 10^{15-16}$ s^{-1}. Since the resonant absorption $B_{K\alpha}$ coefficients are related to the $A_{K\alpha}$ coefficients by the factor $(c^3/8\pi h\nu^3)$, we find that the $B_{K\alpha}$ are of the same order of magnitude as the $A(\mathrm{M}\rightarrow\mathrm{L})$. Therefore, the condition implied by eq 2 should be satisfied for sufficiently intense Kα X-ray sources. The X-ray sources mentioned earlier are capable of high Kα photon fluxes; for example, pulsed photon yields of $\approx 10^{8-9}$ for foil targets of Ti to Ta at femtosecond (10^{-15} s) time scales have been obtained.[20] Synchrotron based X-ray sources are capable of high photon fluxes[16] in excess of 10^9.

If the K-shells of neutral gold atoms are ionized to create one- or two-electron vacancies in the L-shell, then Kα resonant excitation can be effected *to the same extent* according to eqs 2 and 3. In that case, the resonant absorption coefficients can be taken to be the same as for F-like and O-like Au ions respectively (Table 1). This should be a reasonable approximation since transition strengths for deep inner shell transitions, especially the K → L, should be largely unaffected by outer-shell electron correlations, and influenced mainly by nuclear charge screening. The total Kα oscillator strengths are approximately independent of Z along a given isoelectronic sequence. Calculations involving eq 2 entail a large number of A and B coefficients and photon fluency rates Φ for high-Z atoms. Some of these data have been computed,[23] and applied to numerical simulations in the accompanying paper by Montenegro et al.[24] in this volume. Next, we sketch the basic atomic calculations for resonant absorption.

Computations

We confine the energy region under study from K-shell excitations up to the K-edge. This refers to K → L, M, N, O, P, etc., or $\Delta E(n = 1 \rightarrow 2, 3, 4, 5, ...)$, up to the 1s ionization energy. The set of resonant K-shell transitions then refers to Kα, Kβ, Kγ, Kδ, Kη, etc. The strongest resonances correspond to sets of $1s \rightarrow np$ dipole transition arrays. For instance, the Kα ($1s \rightarrow 2p$) resonance complexes will manifest themselves in absorption by highly ionized ions of an element from the Hydrogen-like to Fluorine-like ionization states. In previous works we have computed and studied the behavior of Kα transition probabilities in Au ions,[23] and along the fluorine sequence for many elements up to Au.[25] The calculations were carried out using atomic structure codes SUPERSTRUCTURE,[26] the Breit−Pauli **R**-matrix (BPRM) method as employed under the Iron Project,[27] GRASP2,[28] and Dirac−Fock and relativistic coupled cluster (RCC) methods.[29] The results from calculations using these methods agree to within 10−30% for all transitions.[23,25] This level of accuracy is sufficient for demonstrating the efficacy of monochromatic radiation absorption in a plasma, which is orders of magnitude higher than the background, as shown in the next section.

Transition strengths are computed for all possible transitions among fine structure levels SLJ of the K and L-shells. The number of transitions varies widely for each ion from H-like to F-like state. The calculation of plasma attenuation coefficients requires photoabsorption cross sections as functions of incident photon energy. Line or resonance absorption strengths may be extended to incorporate broadening profiles that are energy dependent.[22] Employing the calculated transition rates for the Kα resonances, we compute the resonant photoabsorption cross sections according to[21]

$$\sigma_{K\alpha}(\nu;\mathrm{K}\rightarrow\mathrm{L}_i) = \frac{4\pi^2 a_o{}^2\alpha}{3}\frac{E(K-L_i)}{g_k}S(\mathrm{K}-\mathrm{L}_i)\phi(\nu) \qquad (4)$$

where the L_i refers to the upper level in the open (ionized) L-shell, $E(\mathrm{K}-\mathrm{L}_i)$ is the corresponding energy, and $S(\mathrm{K}-\mathrm{L}_i)$ is the line strength, and the initial level statistical weight $g_K = 1$. The profile factor $\phi(\nu)$ depends on the plasma conditions (temperature-density) and is normalized to unity for each resonance complex (Kα, Kβ, etc.)

$$\int_{\Delta\nu_{res}} \phi(\nu)\, d\nu = 1 \qquad (5)$$

For Fe and Au ions, Table 1 gives the transition arrays, number or resonances N_T, the average Kα energy $E(\mathrm{K}\alpha)$, and $\langle\sigma_{res}(\mathrm{K}\alpha)\rangle$, the total $\Sigma_i\sigma_{res}(\mathrm{K}-\mathrm{L}_i)$ cross section averaged over the Kα energy range $\Delta E_{K\alpha}$. The Kα transition arrays given in Table 1 range over a number of transitions in H-like to F-like ions (described in detail in ref 23). Each transition corresponds to a specific Kα resonance. To provide a rough estimate of the magnitude of this effect, we have grouped these for each ion

and computed a simple average value given in Table 1. These resonance strengths provide the dominant contribution to photoabsorption, far above the background, as discussed in the next section.

Results and Discussion

This section presents results based on the theoretical and computational mechanisms described here. Sample models are also presented for X-ray attenuation as a prelude to more detailed Monte Carlo simulations presented in the accompanying paper in this volume by Montenegro et al.[24]

Resonant Photoabsorption Coefficients. Computation of extinction coefficients requires not only the basic atomic parameters computed above but also knowledge of the target conditions, line or resonance broadening parameters, and related ionic or electron vacancy distributions. We do not consider any specific source, but rather a simplified model of a transient plasma such as might be created by a monochromatic Kα radiation source of sufficient intensity to generate very highly charged high-Z ions. Without loss of generality, we assume a certain line broadening width $\phi(\nu)$ for the K-shell resonances. Using the resonant absorption cross sections for individual transitions within the Kα complex (K → L), eq 4, and similarly for the Kβ, Kγ, Kδ, and Kε complexes corresponding to transitions to the M, N, O, and P, respectively, we compute resonant⊕nonresonant mass attenuation coefficients κ, for different ns,np-subshells in Fe and Au ions (np;n = 3, 4, 5, 6). The resonant cross sections were convolved over a normalized Gaussian function with an arbitrary fwhm = 10 eV for Fe ions, and 100 eV for Au ions, to exemplify the beam width and other broadening effects in the target. The mass attenuation coefficient per volume mass, μ/ρ is related to the total photoabsorption cross section $\sigma_{\rm tot}$ as

$$\kappa = \mu/\rho\ (\mathrm{cm}^2/\mathrm{g}) = \sigma_{\rm tot}/uW_{\rm A} \qquad (6)$$

where ρ is the bulk density, u is 1 amu, and $W_{\rm A}$ is the atomic weight.

Figures 4 and 5 show the monochromatic photoabsorption coefficients for H-like to F-like Fe and Au ions below the K-edge, 7.11 keV for Fe and 80.729 keV for Au. The K-shell resonance complexes are seen to enhance total X-ray absorption by large factors, up to $\sim 10^3$ for Au, and smaller but significant factors ~10 for Fe, at the corresponding energies relative to the background. The background photoionization cross sections including the K-edge have been computed using the relativistic distorted wave approximation.[30] Several common features may be noted in these figures for both elements. If one examines the *cumulative* effects of K-shell absorption in all ions shown, much of the energy region from the Kα resonance complex up to the K-edge could cause considerable X-ray extinction: 6.4−7.1 keV for Fe ions, and 68.7−80.7 keV for Au ions. The total absorption by complexes Kα, Kβ, etc., decreases as n^{-3}. Of particular note, which was not explored before, is the K-ionization jump which is orders of magnitude smaller than resonant cross sections for Au, and smaller (though not as significant) for Fe. Thus, compared to resonant energies, continuum X-ray opacity in the high-energy regime is generally small. It is clear that X-ray intensity attenuation will be quite in contrast at background energies as opposed to resonant complexes, as modeled in the next section.

The main difference between the results for Fe and Au are also apparent from Figures 4 and 5. The background photoabsorption cross sections for Fe are much higher than for Au; a rough scaling is as Z^{-2}. But the resonance absorption strengths remain roughly constant (analogous to line oscillator strengths) for the 1s → 2p complex.[25] Therefore, the resonant to background ratio for Au is much larger than for Fe. In other words, the resonant absorption effect should manifest itself more clearly as Z increases, further emphasizing the advantage of high-Z elements corresponding to high X-ray energies.

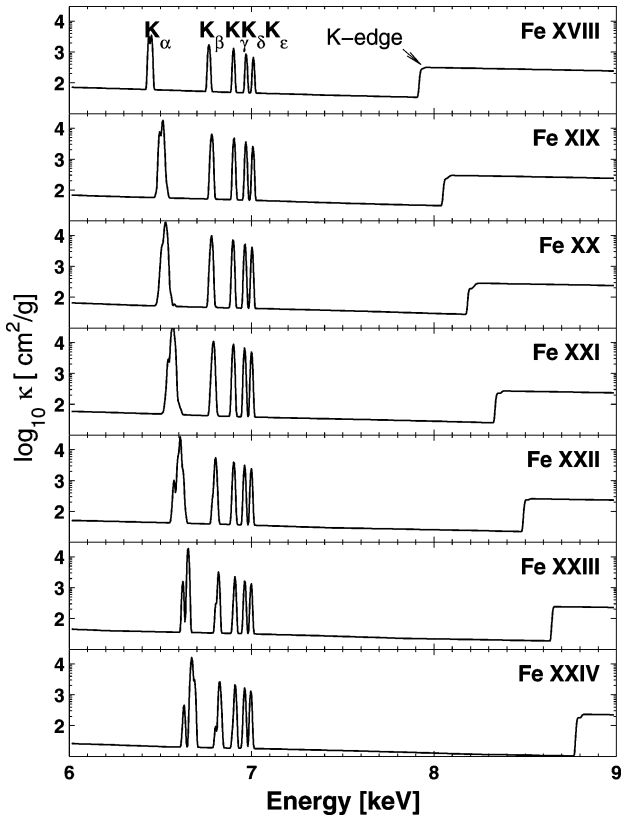

Figure 4. Total resonant K-shell absorption complexes and nonresonant X-ray mass attenuation coefficients κ (cm^2/g) for iron ions. The resonance profiles (eq 4) are assumed to be Gaussian with fwhm = 10 eV. The averaged Kα resonance peaks are more than an order of magnitude higher than the K-edge jumps (the two fine structure components of Kα are unresolved).

Transmitted Intensity. Attenuation of radiation through a plasma depends on temperature, density, and the material. There is no generally applicable methodology that would apply to all physical situations, from low-temperature molecular composition in the body to high-temperature plasmas encountered in laboratory devices. Nor is the problem of line or resonance profile factors in eq 4 under all plasma conditions readily solved quantitatively. Nevertheless, we can make some estimages of the parameter space that describe radiative attenuation in general. More detailed numerical simulations of the monochromatic X-ray intensity propagated through body tissue containing high-Z nanoparticles is described in the accompanying paper by Montenegro et al.[24] Here we note the basic expression that describes the exponential attenuation of radiation intensity in a medium is $I = I_0 \exp[-(\mu/\rho)x]$, where x is the depth and I_0 is the incident intensity in the beam.[15] We express the monochromatic mass attenuation coefficient as $\kappa_\nu \equiv (\mu/\rho)_\nu$, Thus, continuous variation of monochromatic intensity κ_ν is

$$I_\nu(x) = I_0(\nu) \exp[-\rho\kappa_\nu(x)x] \qquad (7)$$

Extinction of X-ray intensity depends explicitly or implicitly on several parameters: the energy (frequency ν), density, and

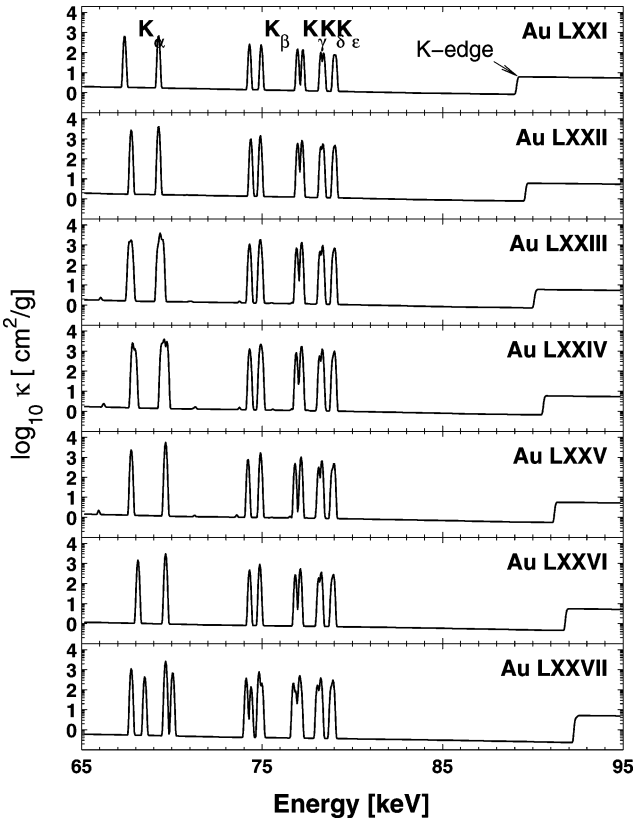

Figure 5. Total resonant K-shell and nonresonant X-ray mass attenuation coefficients κ (cm^2/g) for gold ions. The resonance profiles (eq 4) are assumed to be Gaussian with fwhm = 100 eV. The Kα peak values, averaged over the two fine structure components, are approximately 2 orders of magnitude higher than the K-edge jumps; compared to the background, they are about 3 magnitudes higher.

depth. As we have shown in this paper, there is strong dependence of κ_ν on each ionization stage capable of K-shell excitation. Taking account of the ionization state dependence for K- and L-shell ions, the attenuation coefficient is given by

$$\kappa_{\rm res}(\nu;K\alpha) = [\sum_j w_j \sum_i \sigma_{\rm res}(\nu;{\rm K-L}_{ji})/uA]/\sum_j w_j \quad (8)$$

with w_j as the ionization fraction for an ion core j in the L-shell. For instance, we may carry out simulations of X-ray propagation assuming equipartition between only one and two L-shell vacancies, i.e., excitation of a plasma ionized up to F-like and O-like ions of Fe and Au.

Figures 6 and 7 are twin 3-D plots of X-ray intensity extinction I/I_0 at (i) resonant energies (LHS) and (ii) background energies close to but below the K-edge. Both numerical simulations, for Fe and Au, show considerable extinction at depths $x \ll 1$ cm and densities $\rho \ll 1$ g/cm^3. Examining the results for Fe and Au individually in Figure 6 and Figure 7, respectively, we find resonant X-ray absorption in a parameter space bounded at the lower end by [x (cm), ρ (g/cc)] $\rightarrow$ (10^{-4}, 10^{-3}) for Fe (Figure 6). That implies, for instance for Fe, that at densities as low as 0.001 g/cm^3, resonant extinction of incident intensity falls to nearly zero at depths $<10^{-3}$ cm. Even more so, for Au (Figure 7) the extinction length (depth) is smaller, $<10^{-4}$ cm, at the same density. Otherwise, using background absorption cross sections, the comparisons on the right side of both figures show that there is no significant extinction for lengths shorter than, or densities lower than these values. Since the resonant/background absorption ratio is much smaller for Fe than for Au, the extinction scale lengths for Fe are about 1−2 orders of magnitude larger.

Atomic Clusters and Nanoparticles. Given that a high-Z nanoparticle is an atomic−molecular cluster, Auger decays from a single high-Z atom will lead to a cascade of photon-electron emissions that would impinge upon nearby atoms. Resonance enhancement of the Auger process through induced monochromatic X-ray photoexcitations may also be viewed as the "inverse Auger effect". There is emerging activity in laser ionization of high-Z elements in nanotechnological applications. Laser induced explosions of Au nanoparticles have been studied in various formations and sizes such as spheres, rods, and shell structures.[31] Although the incident laser wavelength is in the optical/infrared range (such as 785 nm in the experiment cited above[31] and 800 nm in ref 32), multiple ionization stages may be created by the so called "Coulomb explosion" scheme.[33] If the laser intensity is sufficiently high, then ionized electrons are accelerated to high energies leading to many secondary ionizations, creating a net positive charge in the targeted atomic cluster which then breaks up due to Coulomb repulsion. Intense laser-cluster interactions can thereby lead to high-energy X-ray generation, with inner-shell vacancies and resulting stimulated X-ray yields.[32,34] The following discussion addresses the complementary issue of X-ray absorption studied in this paper.

Biomedical Applications. In addition to general applications utilizing K-shell X-ray emission and absorption in high-Z elements, we note the possibility of one particular application in biomedical physics. In recent years there has been some work on X-ray irradiation of nanoparticles embedded in malignant body tumors. Depending on the size of nanoparticles, and therefore the number of high-Z atoms, the breakup of a nanoparticle may be quite sufficient to cause single and double strand breakups of the DNA comprising the cell. As mentioned, such breakups due to low-energy electron attachment resonances with DNA at resonant energies have been observed.[10] Using high-Z nanoparticles there is likely to be copious production of low-energy electrons, particularly following Super-Coster−Kronig transitions involving the highest n-shells and subshells. In recent experiments it has been shown that there is considerable reduction in tumor size when embedded gold nanoparticles are subjected to high-energy X-rays from conventional bremsstrahlung sources with 250 kVp (peak voltage).[12,13] A 250 kVp source has peak emission at ~81 keV, close to the Au K-edge (Figure 1). If the tumors are not deeply located, X-ray ionization of much lower energy L-shells (~11−14 keV) may also be effective in the breakup of Au nanoparticles, and consequent destruction of malignant cells.

In general, for medical applications one may need high energies close to the K-shell ionization energies of gold to ensure sufficient penetration. But at very high energies $E \rightarrow 1$ MeV, radiation extinction even by high-Z elements from iron to gold is essentially the same as for low-Z elements such as oxygen. The attenuation coefficients are seen to converge at high energies (Figure 1), and gold is nearly as transparent as oxygen. This demonstrates that high-energy radiation from linear accelerators at $E > 1$ MVp used in medical radiation diagnostics and therapy would *not* exhibit any enhancement due to resonant absorption, being too far above the K-shell energies. It follows that the use of high-Z nanoparticles is also not likely to be very effective if very high energy radiation in the MeV range is utilized. These and other physical scenarios are studied through Monte Carlo numerical simulations elsewhere in this volume in the paper by Montenegro et al.[24]

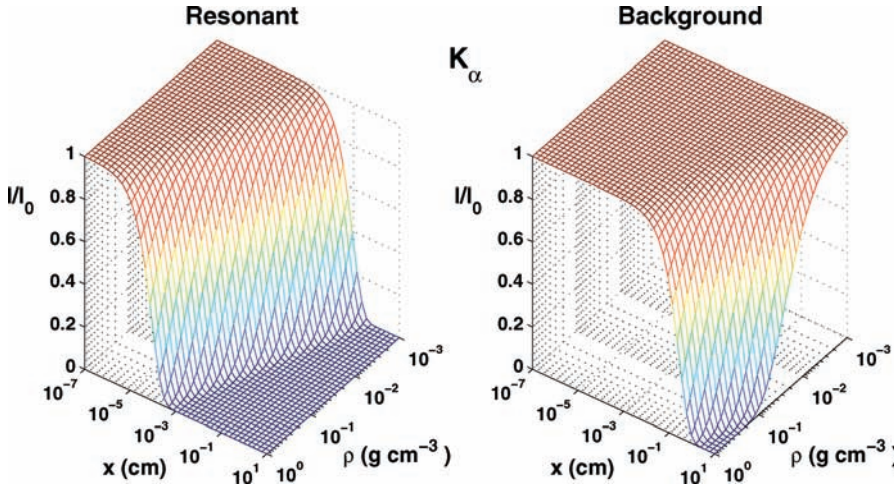

Figure 6. Resonant (LHS) and background (RHS) X-ray extinction via Kα resonances at ~6.4 keV in an iron ion plasma with F-like and O-like ion cores (see text).

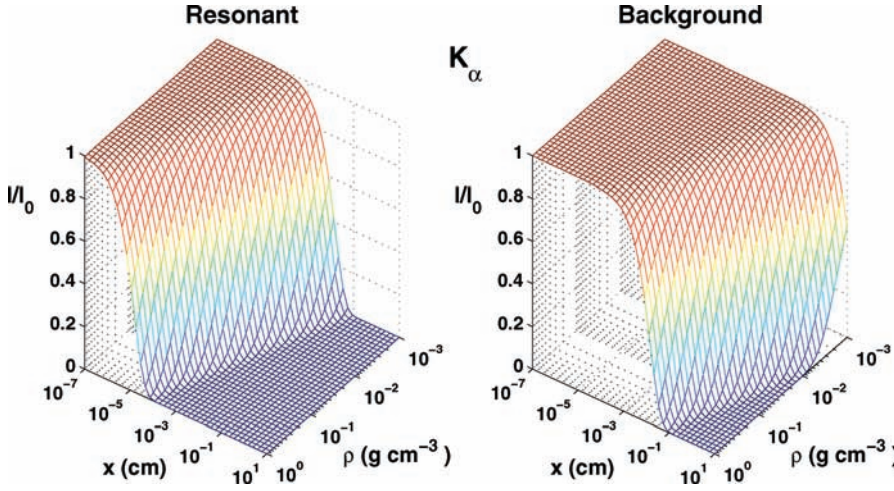

Figure 7. Resonant (LHS) and background (RHS) X-ray extinction via Kα resonances at ~68 keV in a gold ion plasma with F-like and O-like ion cores (see text).

We have noted that K-shell ionization leads to Kα emission with fluorescent efficiency well above 90% owing to high *A* coefficients. Therefore, Kα emission can be readily utilized for imaging diagnostics using monochromatic X-rays rather than broad-band imaging. Whereas high intensities are obviously needed for radiation nanotheranostics to break up high-*Z* nanoparticles, imaging can be carried out with relatively low intensity ionization of K-shells and resultant Kα emission for many elements and compounds, such as BUdR or IUdR. Finally, we emphasize that although the intensities required to implement the Kα resonant excitations may be high, the overall radiation exposure may still be less than what is needed in contemporary X-ray imaging and therapy where most of the incident energy is ineffective.

Conclusion

We have presented a theoretical framework for resonance enhancement of the Auger processes—photon emissions and electron ejections—by external irradiation from monochromatic X-ray source(s) at resonant energies corresponding to inner shell transitions. Resulting line emission, especially the Kα, could be employed for diagnostic imaging with greatly reduced exposure compared to broad-band radiation. The inverse process of resonant excitation into electron vacancies created by Auger decays following K-shell ionization should be particularly effective for therapeutic purposes, in combination with nanoparticle radiosensitization with high-*Z* materials.

Toward that goal, we have analyzed K-shell resonant X-ray absorption in iron and gold atoms with particular attention to the Kα resonance complex. The atomic data for resonance transition strengths are transformed to absorption cross sections to enable numerical simulations of the attenuation of X-ray intensity as function of plasma density and length. It is found that highly ionized ion cores of high-*Z* atoms are highly suitable for efficient energy deposition, provided (i) the incident X-rays are tuned to the resonance complexes, and (ii) sufficient intense monochromatic sources are available (much lower intensities would be needed for imaging via Auger photon emission, than for the inverse process of resonant absorption). These complexes correspond not only to the Kα absorption but also to the higher *n*-complexes up to the K-edge.

Resonant phenomena in neutral atoms or atomic clusters, and radiosensitzed moieties and nanoparticles, may be utilized for biomedical applications when irradiated with X-rays at resonant energies. Electron vacancies in deep inner shells would be filled by upward excitations, given by competing Auger decay rates in such hollow atoms. In particular, the L-shell vacancies are important since they they correspond to Kα emission and excitation whose energy in high-*Z* atoms lies in a range of X-rays that can penetrate to significant depths in the human

body. For example, 68 keV photons can maintain considerable flux up to 10 cms depth (illustrated in simulations in the accompanying paper in this volume by Montenegro et al.[24]). If resonant absorption and emission can be realized, then high-*Z* nanoparticles would be efficient emitters/absorbers of X-rays produced by high-intensity sources, and utilized for medical imaging via Auger fluorescence, or therapy with localized energy deposition and destruction of malignant cells in a tumor. In addition, the Auger decays would also generate secondary ejected electrons that would cause the same effect. This suggestion may be validated experimentally using synchrotron X-ray sources, laser produced plasma sources capable of generating high-intensity monochromatic photon fluxes, and even combination of ordinary broad-band radiation sources used to produce Kα line radiation. Moreover, femtosecond X-ray sources should be available in the future to operate on the same time scales as the rates for radiative and Auger transitions associated with K-shell excitations. Further work on developing this model might be carried out with Monte Carlo simulations incorporating the atomic and molecular processes discussed in the paper by Montenegro et al.[24] in this issue.

In general, biomedical applications involve molecular complexes with high-*Z* atoms. These include commonly used compounds such as BUdR and IUdR, and heavier systems such as cyclo-Pt and carboplatin.[35,36] The use of nanoparticles made of iron or gold is now widespread. However, construction, targeting, and delivery remain one of the main challenges in nanobiotechnology. The essential problem is to coat the nanoparticles with antigen moieties that would target the antiibodies and deposit around or penetrate tumor cells. Considerable future research in nanobiotechnology is needed to realize and maintain a large uptake ratio of injected nanoparticles in the malignant tissue, as opposed to healthy cells elsewhere in the body.

Acknowledgment. This work was partially supported by a Large Interdisciplinary Grant award by the Office of Research, the College of Mathematical and Physical Sciences, and the Department of Astronomy at the Ohio State University. The computational work was carried out at the Ohio Supercomputer Center in Columbus Ohio.

References and Notes

(1) Spiers, W. *Br. J. Radiol.* **1949**, *22*, 512.
(2) Sundararaman, V.; Prasad, M. A.; Vora, R. B. *Phys. Med. Biol.* **1973**, *18*, 208–218.
(3) Larson, D.; Bodell, W. J.; Ling, C.; Phillips, T. L.; Schell, M.; Shrieve, D.; Troxel, T. *Int. J. Radiat. Oncol. Biol. Phys.* **1989**, *16*, 171–176.
(4) Takakura, K. *Radiat. Environ. Biophys.* **1989**, *28*, 177–184.
(5) Howell, R. W. *Int. J. Radiat. Biol.* **2008**, *84*, 959–975.
(6) Nikjoo, H.; Emfietzoglou, D.; Charlton, D. E. *Int. J. Radiat. Biol.* **2008**, *84*, 1011–1026.
(7) Pignol, J.; Rakovitch, E.; Beachey, D.; Le Sech, C. *Int. J. Radiat. Oncol. Biol. Phys.* **2003**, *55*, 1082–1091.
(8) Bernhardt, P.; Friedland, W.; Paretzke, H. *Radiat. Environ. Biophys.* **2004**, *43*, 77–84.
(9) Le Sech, C.; Takakura, K.; Saint-Marc, C.; Frohlich, H.; Charlier, M.; Usami, N.; Kobayashi, K. *Radiat. Res.* **2000**, *153*, 454–458.
(10) Boudaiffa, B.; Cloutier, P.; Hunting, D.; Huels, M.; Sanche, L. *Science* **2000**, *287*, 1658–1660.
(11) Silver, E.; Pradhan, A. K.; Yu, Y. *RT Image* **2008**, *21*, 30.
(12) Hainfeld, J.; Slatkin, D.; Smilowitz, H. *Phys. Med. Biol.* **2004**, *49*, N309–N315.
(13) Cho, S. *Phys. Med. Biol.* **2005**, *50*, N163–N173.
(14) Tsutsui, H.; Ohtsuchi, T.; Ohmori, K.; Baba, S. *IEEE Trans. Nucl. Sci.* **1992**, *39*, 2282–2285.
(15) Physical Reference Data,www.nist.gov/Phys.Ref.Data.
(16) Zhavoronkov, N.; Gritsai, Y.; Bargheer, M.; Woerner, M.; Elsaesser, T. *Appl. Phys. Lett.* **2005**, *86*, 244107.
(17) Andiel, U.; Eidmann, K.; Witte, K. *Phys. Rev. E* **2001**, 63. art. no.-026407.
(18) Moribayashi, K.; Sasaki, A.; Zhidkov, A. *Phys. Scr.* **2001**, *T92*, 185–187.
(19) Berger, M.; Motz, J. *Nucl. Instrum. Methods Phys. Res. Sect. B* **2004**, *226*, 327–344.
(20) Reich, C.; Gibbon, P.; Uschmann, I.; Forster, E. *Phys. Rev. Lett.* **2000**, *84*, 4846–4849.
(21) Opacity Project Team. *The Opacity Project*; Institute of Physics Publishing: Bristol, U.K., 1995.
(22) Seaton, M. J.; Yu, Y.; Mihalas, D.; Pradhan, A. K. *Mon. Not. R. Astron. Soc.* **1994**, *266*, 805–828.
(23) Nahar, S. N.; Pradhan, A. K.; Sur, C. *J. Quant. Spectrosc. Radiat. Transfer* **2008**, *109*, 1951–1959.
(24) Montenegro, M.; Nahar, S. N.; Pradhan, A. K.; Huang, K.; Yu, Y. *J. Phys. Chem. A*, DOI: 10.1021/jp905323y.
(25) Sur, C.; Nahar, S. N.; Pradhan, A. K. *Phys. Rev. A* **2008**, *77*, 1.
(26) Eissner, W. *The Effect of Relativity on Atoms, Molecules, and the Solid State*; Plenum Press: New York, 1991.
(27) Hummer, D. G.; Berrington, K. A.; Eissner, W.; Pradhan, A. K.; Saraph, H. E.; Tully, J. A. *Astron. Astrophys.* **1993**, *279*, 298–309.
(28) Parpia, F.; Fischer, C.; Grant, I. *Comput. Phys. Commun.* **1996**, *94*, 249–271.
(29) Sur, C.; Chaudhuri, R. K. *Phys. Rev. A* **2007**, *76*, 12509.
(30) Zhang, H. L. *Phys. Rev. A* **1998**, *57*, 2640–2650.
(31) Letfullin, R. R.; Joenathan, C.; George, T. F.; Zharov, V. P. *Nanomedicine* **2006**, *1*, p473–480.
(32) Lamour, E.; Prigent, C.; Rozet, J.; Vernhet, D. *Nucl. Instrum. Methods Phys. Res. Sect. B* **2005**, *235*, 408–413.
(33) Wabnitz, H.; et al. *Nature* **2002**, *420*, 482–485.
(34) Deiss, C.; Rohringer, N.; Burgdorfer, J.; Lamour, E.; Prigent, C.; Rozet, J.; Vernhet, D. *Phys. Rev. Lett.* **2006**, *96*, 13203.
(35) Kobayashi, K.; Usami, N.; Sasaki, I.; Frohlich, H.; Le Sech, C. *Nucl. Instrum. Methods Phys. Res. Sect. B* **2003**, *199*, 348–355.
(36) Rousseau, J.; Barth, R. F.; Moeschberger, M. L.; Elleaume, H. *Int. J. Radiat. Oncol. Biol. Phys.* **2009**, *73*, 530–536.

JP904977Z